TU Delft

Delft University of Technology

Faculty of Aerospace Engineering

Memorandum M-844

Preliminary Study of a Plug Nozzle Model in Supersonic Flow

W.J. Bannink, E.M. Houtman and M.M.J. Schoones

April 1998

SUMMARY

Nozzle base pressure measurements and flow visualization results are presented for plug nozzle models with a 6x100 mm throat and plug lengths of 30% and 40% referenced to the full plug length. The model was mounted in supersonic free streams of Mach 1.5 and 3.0 produced by the Delft University supersonic wind tunnel ST-15. Measurements without a supersonic free stream were conducted as well. The jet exhausting from the nozzle had a design Mach number of 4.16 and operated at various jet stagnation pressures, such as to have different jet exit pressure to ambient flow pressure ratios. The tilt angle of the nozzle throat was $\Theta = 67.84°$ and the ratio of exit area to throat area at design conditions was $A_e/A_t = 12.35$. Starting with a high value the jet stagnation pressure was reduced during a run in order to study the transition from the 'closed wake' state to the 'open wake' state. Two different phenomena cause changes in the nozzle base pressure curves: 1) the 'closed wake'-'open wake' transition, and 2) the envelope shock moving onto the plug. The flow phenomena encountered were visualized. The present investigation was part of a joint computational/experimental research program on plug nozzle flow physics.

CONTENTS

LIST OF SYMBOLS

A_e	nozzle exit area (mm^2)
A_t	nozzle throat area (mm^2)
D^*	nozzle throat diameter (mm)
L_{pl}	plug length (mm)
M	Mach number
M_d	design Mach number
M_∞	free stream Mach number
p	static pressure
p_{b_i}	nozzle base pressure at pressure tap i
p_t, p_{t_∞}	wind tunnel stagnation pressure
p_{t_j}	jet stagnation pressure
p_∞	free stream static pressure
x	streamwise cooidinate, $x = 0$ at position of vehicle base
y	lateral coordinate, $y = 0$ at model vertical symmetry plane
z	coordinate pointing upwards, $z = 0$ at corner vehicle base
Θ	tilt angle nozzle throat

1. INTRODUCTION

A linear external expansion or plug nozzle engine uses an exhaust nozzle that can be thought of as a conventional bell shaped nozzle turned inside-out. The plug nozzle is a truncated version of an ideal plug. Truncating the ideal plug results in a wake at the base which has some performance loss.

In a bell nozzle propellant gases expand through a converging-diverging nozzle and the diverging walls of the nozzle constrain the expansion away from the centerline. Bell nozzles are a point design with optimum performance at one specific ambient pressure (i.e., altitude). Careful design is needed to achieve desired high altitude performance while avoiding flow separation at the walls of the nozzle near the exit when operating at low altitudes, which can lead to loss of performance and possible structural failure of the nozzle due to dynamic loads. Therefore a compromise altitude must be used for the design point of a bell nozzle.

The plug nozzle offers a solution to this problem. One side of the supersonic expansion is a centerbody or plug, the other side is a free streamline. The flow is directly exposed to ambient pressure and its expansion is thus directly coupled to the external environment (continuous altitude compensation with no moving parts). A sketch of the flow field physics of a plug nozzle with co-flowing supersonic stream can be found in Fig. 1. At low altitude the expansion of the exhaust gas is restricted by the surrounding ambient pressure. A shock wave (the envelope shock) forms on the plug, raising the engine exhaust pressure to match the surrounding ambient pressure. As altitude increases, the ambient air pressure is reduced, the exhaust expands further, and the shock wave moves down the plug. Eventually, at high altitude, it moves off the plug altogether. Thus, a very high area ratio nozzle (high vacuum performance) can also operate efficiently and safely at sea-level.

Subsequently, plug nozzles have two attractive features that satisfy requirements of minimization of vehicle weight and maximization of engine thrust performance: altitude compensation of thrust and better utilization of vehicle base area. However, airflow over the base of the vehicle can result in pressure below ambient at the nozzle exit, causing the nozzle to overexpand, with a resultant performance loss. This loss is most pronounced when the engine is operating near transonic Mach numbers. Furthermore, an undesirable operating condition is found when the envelope shock impinges on the plug contour: it not only causes flow separation, but also causes the heat flux to peak. Again, carefull design is needed to avoid flow separation.

The present study concerns experiments on a linear plug nozzle (or 2D plug nozzle) placed in a supersonic flow. The effect of the free stream Mach number M_∞ and the pressure ratio of jet stagnation pressure to free stream static pressure (p_{t_j}/p_∞) on the nozzle base flow physics was determined. At the nozzle base a subsonic region, bounded by a shear layer (the inner shear layer), and a shock wave (the trailing shock) are formed (Fig. 1). Surface pressures at the nozzle base were measured and Schlieren recordings of the flow field past and behind the body were made. The series of experiments may be considered as preliminary in order to define a more detailed model configuration with a number of pressure taps along the plug, the vehicle base and the nozzle base. Also the proper design of the exhaust dimensions was part of the objectives.

2. EXPERIMENTAL APPARATUS

2.1 Wind Tunnel

The ST-15 supersonic wind tunnel of the Faculty of Aerospace Engineering is a blow down facility with fixed interchangeable blocks. When operated at Mach 3 its test section is 15cm x 15cm and at Mach 1.5 the height of the test section has increased to 20cm. Due to its long running time - a total running time of the order of 18 minutes is available before recharging of the pressure vessel is required - the wind tunnel is still very much in demand for tests involving flow visualization or detailed exploration of the flow field. The possibility of using specially adapted liners has proved to be an advantage for particular tests, as shown in the present configuration depicted in Fig. 3.

2.2 Model Geometry

The selected geometry is symmetric with respect to the x, z-plane and uses the full width of the test section, 15cm. The co-ordinate system used in the x, z-plane can be seen in Fig. 2. The model, shown in Fig. 4, has an overall height of 91.96mm and the distance from the nozzle throat-plug intersection to the lower tunnel wall is 71.84mm. The nozzle throat diameter is $D^* = 6$mm and the width of the nozzle throat is such that only the central 100mm of the test section width is covered. The tilt angle of the nozzle throat is $\Theta = 67.84°$ and the ratio of exit area to throat area at design conditions is $A_e/A_t = 12.35$. The maximum mass flow through the nozzle was restricted to 2.7 kg/s because of structural design reasons. The expansion is being controlled by a nozzle lip at the lower end of the vehicle base (Fig. 1).

The plug is a solid boundary substituting a streamline from a Prandtl-Meyer expansion (simple wave) at the nozzle lip. A perfect plug may be obtained by terminating the solid boundary at the point where it is intersected by a characteristic line and where the expansion has proceeded to just the desired pressure ratio. In other words, a single streamline, cut at the proper point, gives the shape of the supersonic plug contour for any specified pressure ratio. The plug nozzle was designed for a Mach number of $M_d = 4.16$. Thus, a full plug, i.e., from the nozzle throat-plug intersection to the lower tunnel wall, would have a plug length of $L_{pl} = 304.8$mm. Plug lengths of 30% and 40% of the full plug length were used. The model has a free vehicle base and nozzle base. Further details of the model are shown in Fig. 4. Details on plug nozzle design can be found in [1] and [2].

Fig. 5 shows the distribution of pressure taps at the nozzle base. For both plug lengths of 30% and 40% 3 pressure taps were provided at the nozzle base in order to study the effect of the free stream Mach number M_∞ and the pressure ratio of jet stagnation pressure to free stream static pressure (p_{t_j}/p_∞) on the nozzle base flow physics. The different locations were used to check the two-dimensionality of the base flow, which may be indicated by the influence of the lateral direction on the base pressure. The exact location of the pressure taps is given in Tables 1 and 2. The surface pressures were measured using a Druck Ltd PDCR-22, 0-15 psi differential pressure transducer mounted in a Scanivalve.

3. EXPERIMENT DESCRIPTION

3.1 Transition Closed Wake - Open Wake

The experiments were set up to investigate the transition of the nozzle base flow from the 'closed wake' state to the 'open wake' state. Fig. 1 shows a sketch of the flow field physics of a plug nozzle with co-flowing supersonic stream. The primary flow from the plug nozzle expands down the plug surface and then around the corner at the end of the plug. A recirculation region develops at the nozzle base. Within the shear layer the subsonic region is bounded by the nozzle base and the sonic line of the base region. On the outboard side of the plume, the flow expands to match the static pressure of the expanded free stream. At the vehicle base a subsonic region is present, bounded by the jet boundary and the outer shear layer. The jet plume compresses the free stream, causing the formation of a plume shock. Expansion waves from the nozzle lip are reflected from the plug contour as expansion waves and then from the jet boundary as compression waves [3]. The compression waves will coalesce, developing an envelope shock. The altitude compensation characteristics of the plug nozle are directly related to the position of these compression waves in the flow [5].

At high ambient pressures the jet boundary is close enough to the nozzle (the plume does not significantly expand) for the compression waves to strike the nozzle contour and the inner shear layer. The nozzle base pressure is increased by the compression waves impinging on the inner shear layer bounding the subsonic region at the nozzle base. As the ambient pressure decreases, the jet boundary moves outward such that the compression waves and/or envelope shock move down the nozzle contour. The nozzle base pressure remains under the influence of ambient pressure as long as the compression waves impinge on the inner shear layer bounding the subsonic region. Once the compression waves move downstream of the sonic line of the nozzle base flow additional decreases in ambient pressure have no further effect on nozzle base pressure [4]. The plug nozzle is in the 'closed wake' regime as the nozzle base pressure is insensitive to ambient pressure. Prior to this point, when the nozzle base pressure is sensitive to ambient pressure, the plug nozzle is in the 'open wake' regime. Altitude compensation affects the nozzle thrust only during the 'open wake' regime.

3.2 Description

The measurements were performed at free stream Mach numbers of $M_\infty = 1.5$ and 3.0 and at wind tunnel stagnation pressures of $p_t = 2.6$ and 6.2 bar, respectively. Measurements were also performed with plug nozzle flow only and a surrounding pressure of 1.0 bar. These values are nominal values. For the case without free stream the jet operated as an ejector, decreasing the surrounding pressure. Wind tunnel stagnation pressures ranging from $p_t = 0.6$ to 1.0 bar were found during a run. Two series of measurements were made: one with a plug length of 30% and one with a plug length of 40%, both referenced to the full plug length. The jet stagnation pressure was varied between 1 and 20 bar. Starting at a high jet stagnation pressure the pressure was reduced during a run with a step interval of about 0.5 bar. At each separate stage surface pressure measurements were conducted with 10 samples for each pressure transducer. The test matrix is given in Table 3. Schlieren video recordings were taken of each test.

4. RESULTS

4.1 $M_\infty = 0$, Nozzle Base Pressures and Schlieren Results

Figures 6 and 7 show the nozzle base pressure curves for a plug length of 30% for the case of no free stream. Table 4 shows the tabulated data. All three ports are depicted in the same figure for comparison. A negligible difference in nozzle base pressure is found for the different ports. Thus, it can be concluded that the base flow in the central part of the model is two-dimensional, the verification of it being the reason for the lateral pressure tap positions. A 'closed wake' state would show a constant p_b/p_{t_j} in the p_b/p_{t_j}-p_{t_j}/p_∞ curve, since the nozzle base pressure is insensitive to ambient pressure for this state. Fig. 6 does not show a constant p_b/p_{t_j}, suggesting that the 'closed wake' state was not reached. However, the Schlieren recordings show that the 'closed wake' was reached for a small range of jet stagnation pressures, ranging from about $p_{t_j}/p_\infty = 23$ to $p_{t_j}/p_\infty = 30.6$. Fig. 7 shows the place of transition from the 'closed wake' state to the 'open wake' state; at about $p_{t_j}/p_\infty = 23$, where the nature of the pressure curve changes. The Schlieren recordings show that here the transition takes place. Fig. 7 also shows that the nozzle base produces drag for the complete range of jet stagnation pressures, since the base pressure is less than the free stream static pressure.

Figures 8 and 9 show the nozzle base pressure curves for a plug length of 40% for the case of no free stream. Table 5 shows the tabulated data. Again, the nozzle base pressure is independent of the position of the pressure tap. Fig. 8 shows that the 'closed wake' state was reached, but only for a small range of jet stagnation pressures, ranging from approximately $p_{t_j}/p_\infty = 26$ to $p_{t_j}/p_\infty = 30.4$. The transition from the 'closed wake' state to the 'open wake' state is found at about $p_{t_j}/p_\infty = 26$. The limitation of the jet stagnation pressure prohibits a proper study of the 'closed wake' regime. Fig. 9 shows that, again, the nozzle base produces drag for the complete range of jet stagnation pressures.

Schlieren photographs are shown in Figures 10 and 11 for the cases of no free stream and plug lengths of 30% and 40%, respectively. Fig. 10 shows a 'closed wake' state. This photograph is taken in the regime where the flow alternates between the 'closed wake' state and the 'open wake' state. The actual transition appears to occur by alternating between both states. Fig. 11 is taken in the 'open wake' regime. The jet boundary, the envelope shock, the inner shear layer and the subsonic region at the nozzle base are visible (see Fig. 1 for an explanation of the different terms). In the photographs the jet boundary is represented by the black layer and the envelope shock by the white layer. In both Figures 10 and 11 the envelope shock impinges on the plug. In both cases separation of the flow at the plug is present and the jet boundary interacts with the separated flow.

4.2 $M_\infty = 1.5$, Nozzle Base Pressures and Schlieren Results

In Figures 12 and 13 the nozzle base pressure curves for a plug length of 30% at $M_\infty = 1.5$ are shown. The tabulated data are given in Table 6. For a ratio of jet stagnation pressure to free stream static pressure, ranging from about 13 to 22, a considerable fluctuation in nozzle base pressure is found. This fluctuation is caused by the interaction of the shear layer originating at the corner of the vehicle base and the jet boundary. This interaction shows an instability effect related to the vehicle base pressure. A clear description can be given for the case of $M_\infty = 1.5$ and a plug length of 40%, which will be

discussed later. Due to the instability effect and the limitation in jet stagnation pressure the 'closed wake' state was not reached.

Fig. 14 shows Schlieren photographs for the case of $M_\infty = 1.5$ and a plug length of 30%. In Fig. 14a a high ratio of jet stagnation pressure to free stream static pressure is shown. The vehicle base pressure is too high for the shear layer originating at the vehicle base to form a closed subsonic region at the vehicle base with the jet boundary. Compression waves coming from the shear layer coalesce into a shock wave (black streak at top right in Fig. 14) which reflects at the tunnel wall. Fig. 14b shows a Schlieren photograph at a ratio p_{t_j}/p_∞ of about half the preceding case, the instability effect is no longer present. The envelope shock impinges on the inner shear layer. The transition from the 'closed wake' state to the 'open wake' state could not be visualized.

In Figures 15 and 16, for a plug length of 40% at $M_\infty = 1.5$, again, a fluctuation in nozzle base pressure is present, however, this time for a smaller range of jet stagnation pressures. The beforementioned instability effect can be visualized by Schlieren photographs at separate stages of the pressure curves. The characters A, B and C depict positions at which these photographs were taken. Table 7 gives the numerical data for this case.

Figures 17a and 17b show Schlieren photographs for the case of $M_\infty = 1.5$ and a plug length of 40%, at a ratio of p_{t_j}/p_∞ where the instability effect occurs. The flow alternates from the state of Fig. 17a to that of Fig. 17b and vice versa. A relatively high vehicle base pressure drives the shear layer and the jet boundary apart, thus decreasing the vehicle base pressure. Then, the decreased vehicle base pressure allows the shear layer and the jet boundary to approach each other, thus increasing the vehicle base pressure. This way the flow alternates between both states. Figures 17c and 17d show Schlieren photgraphs where the instability effect is no longer present. The envelope shock impinges on the plug. Once more, the transition from the 'closed wake' state to the 'open wake' state could not be visualized.

4.3 $M_\infty = 3.0$, Nozzle Base Pressures and Schlieren Results

In Figures 18 and 19 the nozzle base pressure curves are shown for a plug length of 30% at $M_\infty = 3.0$, see also Table 8. Fig. 18 shows that the 'closed wake' state was reached and the transition from the 'closed wake' state to the 'open wake' state could be visualized. This transition occurs at $p_{t_j}/p_\infty = 49$. The 'closed wake' state is present at design conditions for the plug nozzle and generally a closed wake produces a lot of drag, which is not desirable. The 'open wake', on the other hand, can produce thrust. Altitude compensating effects are related to the state of the wake, or more directly: to the position of compression waves in the flow [5]. In the 'closed wake' state a constant ratio of $p_b/p_{t_j} = 0.0037$ is found. Around approximately $p_{t_j}/p_\infty = 35$ a sudden increase in the pressure curves (as seen from right to left; while reducing jet pressure) is present. The nozzle base starts to produce thrust, below approximately $p_{t_j}/p_\infty = 38$ ('open wake' regime). For the remaining part of the pressure curve drag is produced by the nozzle base. The course of the pressure curves can be explained by Schlieren photographs of the flow field at separate stages.

Fig. 20 shows Schlieren photographs for the case of $M_\infty = 3.0$ and a plug length of 30%. Again, characters depict positions at which these photographs were taken. Fig. 20a depicts the 'closed wake' regime. The plume shock, the jet boundary, the envelope shock, the inner shear layer and the trailing shock are visible. The transition from the 'closed wake' state to the 'open wake' state may be observed in Figures 20b and 20c. At this point the flow alternates between both states. Figures 20d

and 20e show the phenomenon which causes the above-mentioned sudden increase revealed in the pressure curves. The envelope shock moves onto the plug, causing a rise in nozzle base pressure. Finally, Fig. 20f shows a Schlieren photograph in the 'open wake' regime. The envelope shock impinges on the plug.

The results for a plug length of 40% at $M_\infty = 3.0$ are shown in Figures 21, 22 and Fig. 23 and in Table 8. Port 3 shows a slight difference in nozzle base pressure, compared to ports 1 and 2. However, this only occured during this particular run and no plausible explanation is available. In this case, the transition from the 'closed wake' state to the 'open wake' state occurs at $p_{t_j}/p_\infty = 54$. In the 'closed wake' state a ratio of nozzle base pressure to jet stagnation pressure of about $p_b/p_{t_j} = 0.0031$ and $p_b/p_{t_j} = 0.0044$ is found for ports 1 and 2 and port 3, respectively. Again a sudden rise in the pressure curves is present at around $p_{t_j}/p_\infty = 38$. The course of the pressure curves is similar to the previous case.

The Schlieren pictures in Fig. 23, taken at separate stages, are similar to the previous case.

4.4 Comparison Nozzle Base Pressures

In Fig. 24 a compilation is made of p_b/p_{t_j}-p_{t_j}/p_∞ curves for a plug length of 30% and 40%, respectively, for port 1 at free stream Mach numbers of $M_\infty = 0$, 1.5, and 3.0. Only one port is used because of the insensitivity of the nozzle base pressure to the position of the pressure tap.

For the pressure curves at a lower free stream Mach number the transition from the 'closed wake' regime to the 'open wake' regime occurs at a lower p_{t_j}/p_∞ than for those at a higher free stream Mach number. Also, the p_b/p_{t_j} value in the 'closed wake' regime is higher. All curves follow the same trend and there are three different regimes present. Two different phenomena mark the transition from one regime to another: 1) the transition from the 'closed wake' to the 'open wake', and 2) the process of the envelope shock moving onto the plug. Comparing the pressure curves for different plug-lengths at similar flow conditions (Fig. 24c) it is apparent that the curves for $M_\infty = 1.5$ do not show similar values and the curves do not match. This is probably caused by the instability effect, which also causes the pressure to fluctuate. The curves for the 'no free-stream' case do match, except for the 'closed wake' regime. The reason for this is that for the plug-length of 30% the 'closed wake' state could not be accurately reproduced. The curves for $M_\infty = 3.0$ match and show that the transition from the 'closed wake' state to the 'open wake' state is found at a lower p_{t_j}/p_∞ for a shorter plug-length, as could be expected.

5. CONCLUSIONS AND RECOMMENDATIONS

Experimental results of a plug nozzle plume with a high supersonic design Mach number of 4.16 exhausting in quiescent air and supersonic free stream flows of Mach 1.5 and 3.0 have been presented for a number of conditions, ranging from $p_{t_j}/p_\infty = 30.6$ to 2.7 at quiescent air, from $p_{t_j}/p_\infty = 35.0$ to 3.8 at Mach 1.5 and from $p_{t_j}/p_\infty = 107.7$ to 15.6 at Mach 3.0. Plug lengths of 30% and 40% referenced to the length of full plug were used. The tilt angle of the nozzle throat is $\Theta = 67.84°$.

The data consists of surface pressure measurements at the nozzle base and Schlieren recordings of all cases tested; video tapes are available. The effect of the free stream Mach number M_∞ and the pressure ratio of jet stagnation pressure to free stream static pressure (p_{t_j}/p_∞) on the nozzle base flow physics has been determined. The transition from the 'closed wake' state to the 'open wake' state has been realised.

Future plans for this program include surface pressure measurements at the plug, vehicle base, nozzle base and downstream of the nozzle base, flow visualization in particular at the plug (oil flow) and in the region directly downstream of the nozzle base (optical). The surface pressure measurements at the vehicle base should clarify the instability effect at $M_\infty = 1.5$. The flow visualizations should shed light on flow separation and on the mechanism of transition of the 'closed wake' state to the 'open wake' state. Because of limitations due to structural design reasons which dictate the maximum mass flow through the nozzle a model with a smaller nozzle throat diameter will be used. This way, the nozzle throat can utilize the full width of the model. Finally, from the comparison of the nozzle base pressures it follows that it is desirable to reach higher values of (p_{t_j}/p_∞).

REFERENCES

[1] Angelino, G., 'Theoretical and Experimental Investigation of the Design and Performance of a Plug-type Nozzle', VKI TN-12, Von Kármán Institute for Fluid Dynamics, Rhode-Saint-Genèse, Belgium, 1963.

[2] Angelino, G., 'Approximate Method for Plug Nozzle Design', Technical Notes, AIAA Journal, Vol. 2, No. 10, 1964.

[3] Martinez, A., 'Interim Report. Aerodynamic Nozzle Study. Volume 2.' Rockwell International Corporation. Rocketdyne Division. Report R-6273, NASA Report CR-68910, 1965.

[4] Ruf, J.H. and McConnaughey, P.K., 'The Plume Physics Behind Aerospike Nozzle Altitude Compensation and Slipstream Effect', AIAA Paper 97-3218, 1997.

[5] Silver, R., 'Final Report. Advanced Aerodynamic Spike Configurations: Volume 1, Analytical and Cold Flow Studies.' Rockwell International Corporation. Rocketdyne Division, Report AFRPL-TR-67-246-Vol I, 1967.

Nr.	x (mm)	y (mm)	z (mm)
1	83.92	0.00	-77.53
2	83.92	-12.00	-77.53
3	83.92	-24.00	-77.53

Table 1: Positions of Static Pressure Taps, 30% Plug-length

Nr.	x (mm)	y (mm)	z (mm)
1	114.40	0.00	-84.06
2	114.40	-12.00	-84.06
3	114.40	-24.00	-84.06

Table 2: Positions of Static Pressure Taps, 40% Plug-length

M_∞	plug length	p_{t_∞} (bar)	p_{t_j} (bar)	p_{tj}/p_∞
0	30%	0.6 – 1.0	18.9 – 2.7	30.6 – 2.7
0	40%	0.6 – 1.0	18.8 – 2.7	30.4 – 2.7
1.5	30%	2.6	18.1 – 2.7	26.0 – 3.8
1.5	40%	1.7	15.9 – 2.6	35.0 – 5.8
3.0	30%	6.2	18.2 – 2.6	107.7 – 15.6
3.0	40%	6.2	15.6 – 3.1	92.8 – 18.5

Table 3: Test Matrix

p_{t_∞} (bar)	p_∞ (bar)	p_{t_j}/p_∞	p_{b_1}/p_{t_j}	p_{b_2}/p_{t_j}	p_{b_3}/p_{t_j}
0.62	0.62	30.6	0.027	0.025	0.026
0.63	0.63	28.9	0.028	0.027	0.027
0.64	0.64	28.0	0.029	0.028	0.028
0.65	0.65	26.7	0.030	0.029	0.029
0.66	0.66	25.9	0.030	0.030	0.030
0.66	0.66	24.9	0.031	0.031	0.031
0.67	0.67	24.0	0.032	0.032	0.031
0.68	0.68	23.0	0.033	0.033	0.033
0.69	0.69	22.0	0.035	0.034	0.035
0.71	0.71	20.8	0.038	0.037	0.038
0.73	0.73	19.8	0.041	0.041	0.041
0.74	0.74	18.7	0.045	0.045	0.044
0.75	0.75	18.0	0.047	0.047	0.046
0.76	0.76	17.1	0.050	0.049	0.048
0.77	0.77	16.3	0.053	0.052	0.051
0.78	0.78	15.5	0.056	0.055	0.055
0.79	0.79	14.8	0.059	0.058	0.058
0.80	0.80	14.0	0.064	0.063	0.062
0.81	0.81	13.4	0.068	0.066	0.066
0.82	0.82	12.6	0.073	0.071	0.071
0.83	0.83	12.0	0.077	0.075	0.076
0.84	0.84	11.4	0.082	0.080	0.080
0.85	0.85	10.7	0.087	0.086	0.085
0.87	0.87	10.0	0.092	0.092	0.091
0.88	0.88	9.4	0.096	0.096	0.096
0.88	0.88	8.8	0.102	0.101	0.102
0.89	0.89	8.3	0.109	0.108	0.109
0.90	0.90	7.7	0.118	0.118	0.117
0.92	0.92	7.1	0.128	0.128	0.128
0.93	0.93	6.5	0.141	0.142	0.142
0.94	0.94	6.1	0.154	0.154	0.154
0.95	0.95	5.5	0.168	0.167	0.169
0.95	0.95	5.1	0.184	0.183	0.184
0.96	0.96	4.5	0.209	0.208	0.209
0.97	0.97	4.1	0.230	0.230	0.230
0.98	0.98	3.6	0.266	0.266	0.266
0.99	0.99	3.1	0.304	0.304	0.304
1.00	1.00	2.7	0.361	0.360	0.361

Table 4: Nozzle Base Pressures, $M_\infty = 0$, 30% Plug-length

p_{t_∞} (bar)	p_∞ (bar)	p_{t_j}/p_∞	p_{b_1}/p_{t_j}	p_{b_2}/p_{t_j}	p_{b_3}/p_{t_j}
0.62	0.62	30.4	0.017	0.017	0.017
0.63	0.63	29.0	0.017	0.017	0.017
0.64	0.64	27.8	0.017	0.017	0.017
0.65	0.65	26.6	0.017	0.017	0.018
0.66	0.66	25.6	0.018	0.018	0.018
0.67	0.67	24.6	0.020	0.019	0.020
0.68	0.68	23.8	0.021	0.020	0.021
0.69	0.69	22.7	0.025	0.025	0.024
0.70	0.70	21.9	0.029	0.028	0.028
0.70	0.70	21.0	0.033	0.032	0.031
0.72	0.72	20.0	0.038	0.036	0.035
0.73	0.73	19.1	0.041	0.038	0.038
0.74	0.74	18.2	0.043	0.040	0.041
0.75	0.75	17.4	0.046	0.043	0.043
0.75	0.75	16.8	0.048	0.045	0.046
0.77	0.77	15.8	0.051	0.049	0.050
0.78	0.78	15.1	0.054	0.052	0.052
0.79	0.79	14.3	0.058	0.055	0.056
0.80	0.80	13.6	0.061	0.060	0.059
0.81	0.81	12.9	0.063	0.062	0.062
0.82	0.82	12.2	0.065	0.064	0.065
0.83	0.83	11.5	0.069	0.067	0.070
0.84	0.84	10.9	0.075	0.073	0.075
0.85	0.85	10.2	0.082	0.080	0.080
0.86	0.86	9.6	0.087	0.085	0.085
0.88	0.88	8.9	0.095	0.094	0.094
0.88	0.88	8.4	0.105	0.104	0.103
0.90	0.90	7.8	0.112	0.111	0.114
0.91	0.91	7.2	0.120	0.117	0.122
0.92	0.92	6.6	0.132	0.131	0.131
0.93	0.93	6.1	0.145	0.145	0.144
0.94	0.94	5.5	0.163	0.163	0.164
0.95	0.95	5.1	0.177	0.177	0.176
0.96	0.96	4.6	0.200	0.201	0.200
0.97	0.97	4.1	0.225	0.225	0.225
0.98	0.98	3.6	0.257	0.258	0.258
0.99	0.99	3.2	0.298	0.298	0.298
1.00	1.00	2.7	0.357	0.357	0.357

Table 5: Nozzle Base Pressures, $M_\infty = 0$, 40% Plug-length

p_{t_∞} (bar)	p_∞ (bar)	p_{t_j}/p_∞	p_{b_1}/p_{t_j}	p_{b_2}/p_{t_j}	p_{b_3}/p_{t_j}
2.56	0.70	26.0	0.043	0.041	0.037
2.56	0.70	25.4	0.043	0.041	0.038
2.56	0.70	24.8	0.044	0.042	0.039
2.56	0.70	24.3	0.045	0.043	0.040
2.56	0.70	23.6	0.046	0.044	0.040
2.56	0.70	22.9	0.047	0.044	0.042
2.56	0.70	22.3	0.048	0.046	0.042
2.56	0.70	21.7	0.048	0.045	0.042
2.56	0.70	21.1	0.048	0.045	0.043
2.56	0.70	20.5	0.049	0.045	0.043
2.56	0.70	19.8	0.048	0.046	0.043
2.56	0.70	19.1	0.047	0.046	0.044
2.56	0.70	18.6	0.048	0.047	0.044
2.56	0.70	18.0	0.047	0.047	0.045
2.56	0.70	17.3	0.049	0.048	0.046
2.56	0.70	16.7	0.051	0.049	0.046
2.56	0.70	16.1	0.051	0.050	0.047
2.56	0.70	15.5	0.051	0.049	0.049
2.56	0.70	14.9	0.053	0.051	0.049
2.56	0.70	14.3	0.050	0.050	0.051
2.56	0.70	13.7	0.049	0.052	0.048
2.56	0.70	13.0	0.050	0.052	0.050
2.56	0.70	12.4	0.052	0.050	0.051
2.56	0.70	11.8	0.054	0.053	0.054
2.56	0.70	11.1	0.057	0.056	0.057
2.56	0.70	10.5	0.060	0.059	0.060
2.56	0.70	9.9	0.064	0.063	0.063
2.56	0.70	9.3	0.067	0.066	0.065
2.56	0.70	8.7	0.072	0.071	0.069
2.56	0.70	8.2	0.075	0.074	0.072
2.56	0.70	7.4	0.082	0.080	0.079
2.56	0.70	6.9	0.087	0.085	0.085
2.56	0.70	6.2	0.094	0.093	0.092
2.56	0.70	5.7	0.100	0.099	0.099
2.56	0.70	5.0	0.109	0.109	0.109
2.56	0.70	4.4	0.122	0.121	0.122
2.56	0.70	3.8	0.140	0.140	0.139

Table 6: Nozzle Base Pressures, $M_\infty = 1.5$, 30% Plug-length

p_{t_∞} (bar)	p_∞ (bar)	p_{t_j}/p_∞	p_{b_1}/p_{t_j}	p_{b_2}/p_{t_j}	p_{b_3}/p_{t_j}
1.67	0.45	35.0	0.033	0.034	0.034
1.67	0.45	33.5	0.034	0.035	0.036
1.67	0.45	32.4	0.034	0.035	0.037
1.67	0.45	31.5	0.034	0.036	0.038
1.67	0.46	30.4	0.035	0.036	0.040
1.67	0.46	29.5	0.035	0.037	0.041
1.67	0.45	28.6	0.036	0.037	0.042
1.67	0.46	27.6	0.037	0.038	0.043
1.67	0.46	26.6	0.038	0.039	0.045
1.67	0.46	25.8	0.038	0.040	0.046
1.67	0.46	24.8	0.039	0.040	0.047
1.67	0.46	23.8	0.039	0.042	0.046
1.67	0.45	22.9	0.039	0.042	0.045
1.67	0.46	21.9	0.041	0.042	0.046
1.67	0.46	21.0	0.040	0.042	0.043
1.67	0.46	20.1	0.040	0.041	0.043
1.67	0.46	19.1	0.043	0.043	0.045
1.67	0.46	18.1	0.045	0.045	0.043
1.67	0.46	17.1	0.042	0.045	0.045
1.67	0.46	16.3	0.047	0.045	0.044
1.67	0.46	15.2	0.050	0.049	0.047
1.67	0.46	14.4	0.055	0.052	0.052
1.67	0.46	13.4	0.060	0.058	0.058
1.67	0.46	12.5	0.067	0.065	0.064
1.67	0.46	11.5	0.074	0.073	0.073
1.67	0.46	10.6	0.084	0.083	0.083
1.67	0.46	9.6	0.096	0.098	0.096
1.67	0.46	8.8	0.112	0.113	0.113
1.67	0.46	7.7	0.132	0.131	0.133
1.67	0.46	6.9	0.154	0.153	0.155
1.67	0.46	5.8	0.188	0.189	0.188

Table 7: Nozzle Base Pressures, $M_\infty = 1.5$, 40% Plug-length

p_{t_∞} (bar)	p_∞ (bar)	p_{t_j}/p_∞	p_{b_1}/p_{t_j}	p_{b_2}/p_{t_j}	p_{b_3}/p_{t_j}
6.21	0.17	107.5	0.0036	0.0036	0.0036
6.19	0.17	106.0	0.0036	0.0036	0.0036
6.18	0.17	103.1	0.0037	0.0036	0.0036
6.18	0.17	100.6	0.0037	0.0036	0.0036
6.18	0.17	97.7	0.0037	0.0036	0.0037
6.18	0.17	95.5	0.0037	0.0036	0.0037
6.19	0.17	92.3	0.0037	0.0036	0.0037
6.19	0.17	90.2	0.0037	0.0036	0.0037
6.19	0.17	87.4	0.0037	0.0037	0.0037
6.19	0.17	84.7	0.0037	0.0037	0.0037
6.19	0.17	81.8	0.0038	0.0037	0.0037
6.19	0.17	79.7	0.0038	0.0037	0.0037
6.19	0.17	77.2	0.0038	0.0037	0.0037
6.19	0.17	74.9	0.0038	0.0037	0.0037
6.19	0.17	71.9	0.0038	0.0037	0.0037
6.19	0.17	69.5	0.0039	0.0038	0.0037
6.19	0.17	66.9	0.0039	0.0038	0.0038
6.19	0.17	64.2	0.0039	0.0038	0.0038
6.19	0.17	61.7	0.0039	0.0038	0.0038
6.19	0.17	59.3	0.0040	0.0039	0.0038
6.19	0.17	56.7	0.0040	0.0039	0.0038
6.19	0.17	53.9	0.0041	0.0040	0.0039
6.19	0.17	51.2	0.0042	0.0041	0.0040
6.19	0.17	48.8	0.0047	0.0046	0.0045
6.19	0.17	46.2	0.0082	0.0078	0.0066
6.19	0.17	43.8	0.014	0.013	0.011
6.19	0.17	41.1	0.017	0.017	0.016
6.19	0.17	38.7	0.022	0.023	0.021
6.19	0.17	35.9	0.040	0.039	0.040
6.19	0.17	33.7	0.045	0.045	0.044
6.19	0.17	30.9	0.052	0.051	0.049
6.19	0.17	28.6	0.058	0.056	0.056
6.19	0.17	25.9	0.069	0.068	0.068
6.19	0.17	23.5	0.078	0.078	0.078
6.19	0.17	20.9	0.091	0.090	0.091
6.19	0.17	18.7	0.103	0.102	0.103
6.19	0.17	15.6	0.129	0.128	0.129

Table 8: Nozzle Base Pressures, $M_\infty = 3.0$, 30% Plug-length

p_{t_∞} (bar)	p_∞ (bar)	p_{t_j}/p_∞	p_{b_1}/p_{t_j}	p_{b_2}/p_{t_j}	p_{b_3}/p_{t_j}
6.19	0.17	92.7	0.0030	0.0029	0.0039
6.19	0.17	90.5	0.0030	0.0030	0.0039
6.20	0.17	87.7	0.0030	0.0030	0.0040
6.19	0.17	85.3	0.0030	0.0030	0.0040
6.19	0.17	82.1	0.0030	0.0031	0.0041
6.20	0.17	79.6	0.0031	0.0031	0.0042
6.20	0.17	77.1	0.0031	0.0031	0.0043
6.20	0.17	74.3	0.0031	0.0031	0.0044
6.20	0.17	71.7	0.0032	0.0032	0.0044
6.20	0.17	69.1	0.0032	0.0032	0.0046
6.20	0.17	66.7	0.0033	0.0033	0.0047
6.20	0.17	64.2	0.0033	0.0033	0.0048
6.20	0.17	61.6	0.0034	0.0034	0.0049
6.20	0.17	59.2	0.0034	0.0035	0.0051
6.20	0.17	56.6	0.0035	0.0035	0.0052
6.20	0.17	54.0	0.0039	0.0040	0.0056
6.20	0.17	51.4	0.0052	0.0052	0.0063
6.20	0.17	49.0	0.0095	0.0085	0.0089
6.20	0.17	46.2	0.014	0.013	0.013
6.20	0.17	43.8	0.018	0.017	0.016
6.20	0.17	43.7	0.018	0.017	0.016
6.20	0.17	41.2	0.022	0.021	0.020
6.20	0.17	38.9	0.028	0.025	0.024
6.20	0.17	36.0	0.040	0.038	0.038
6.20	0.17	33.7	0.045	0.043	0.043
6.20	0.17	31.0	0.050	0.048	0.050
6.20	0.17	28.6	0.058	0.057	0.057
6.20	0.17	25.9	0.064	0.065	0.065
6.20	0.17	23.4	0.073	0.072	0.074
6.20	0.17	20.9	0.084	0.085	0.086
6.20	0.17	18.5	0.102	0.102	0.102

Table 9: Nozzle Base Pressures, $M_\infty = 3.0$, 40% Plug-length

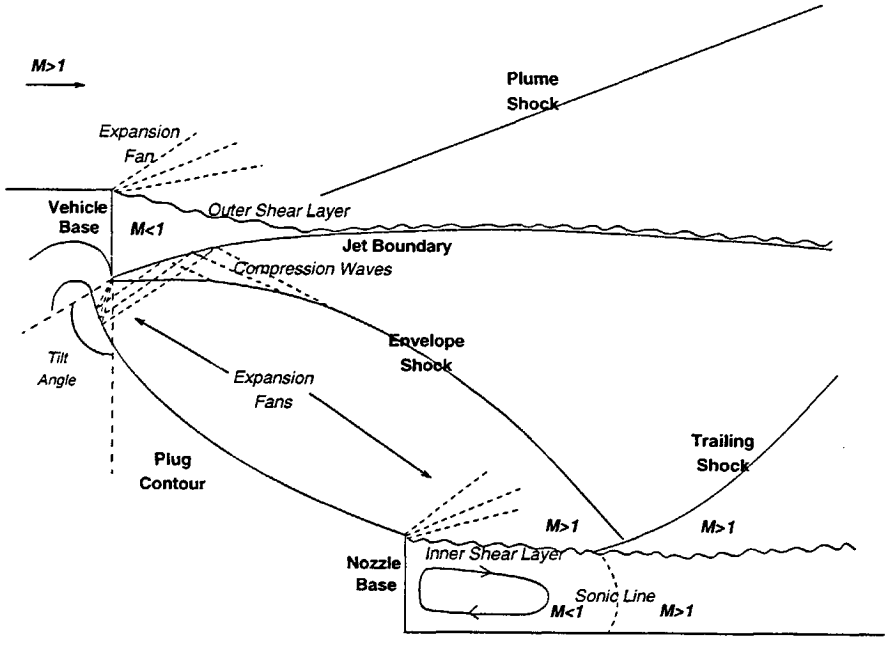

Figure 1: Plume Flow Field for a Plug Nozzle with Co-flow

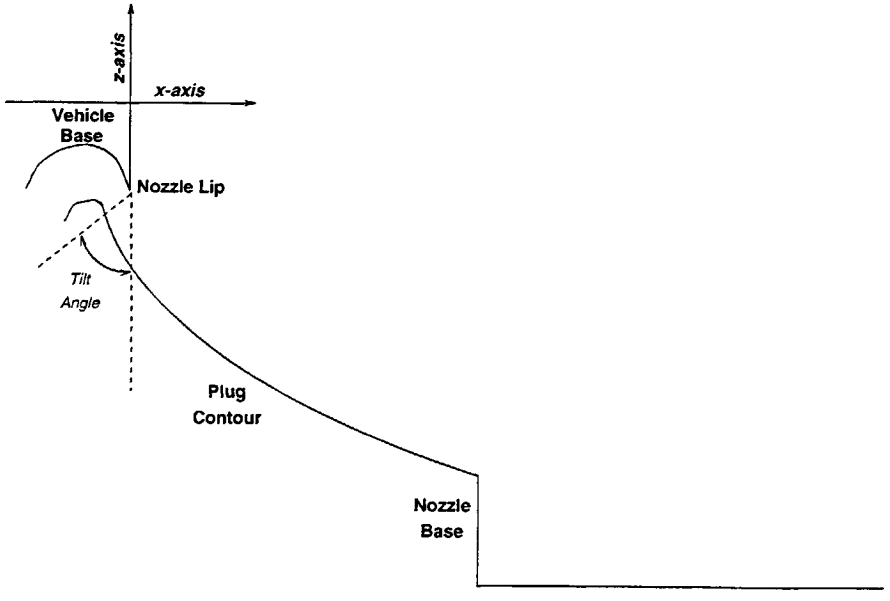

Figure 2: Co-ordinate System in x,z-plane

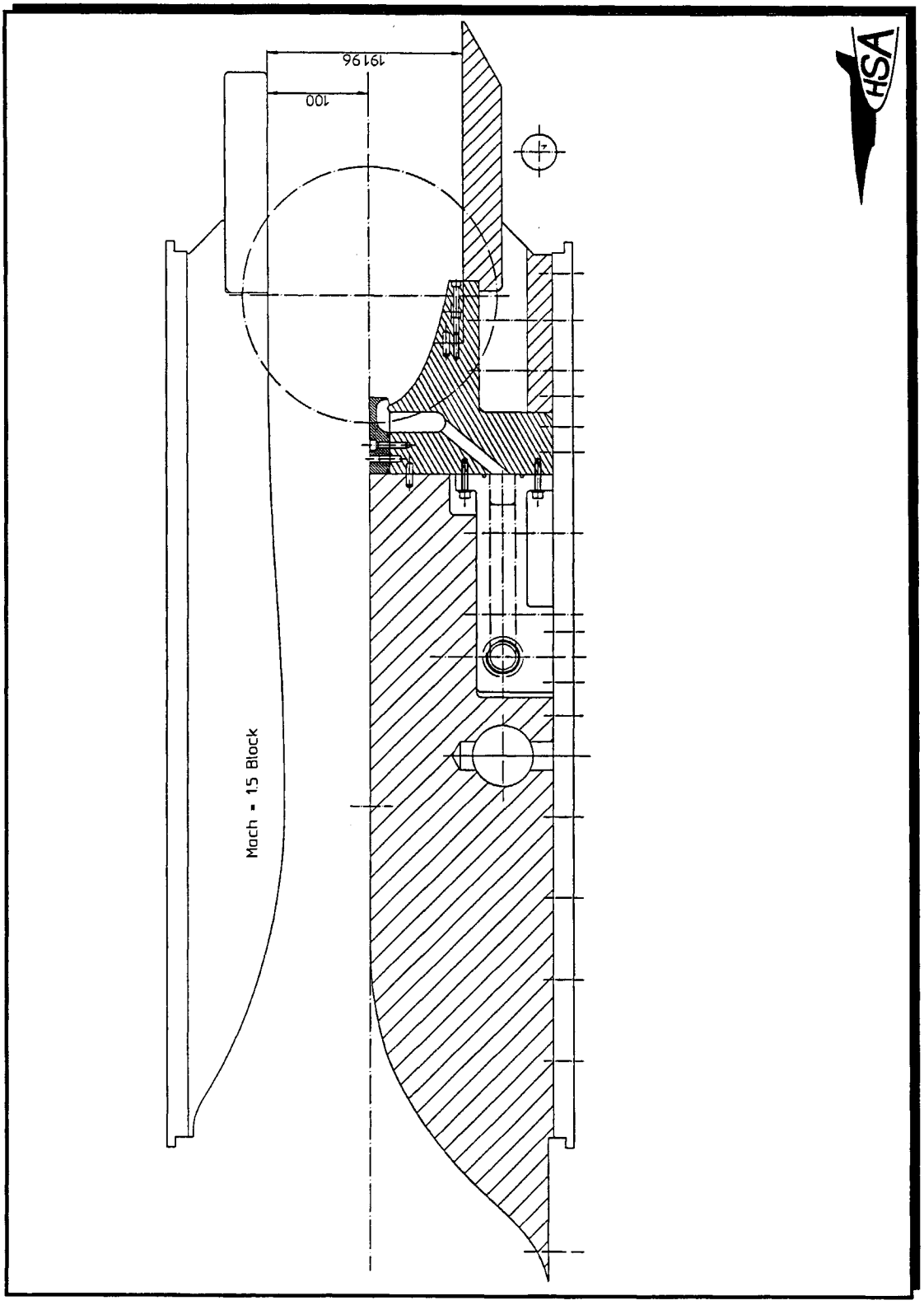

Figure 3: Model Configuration in Wind Tunnel

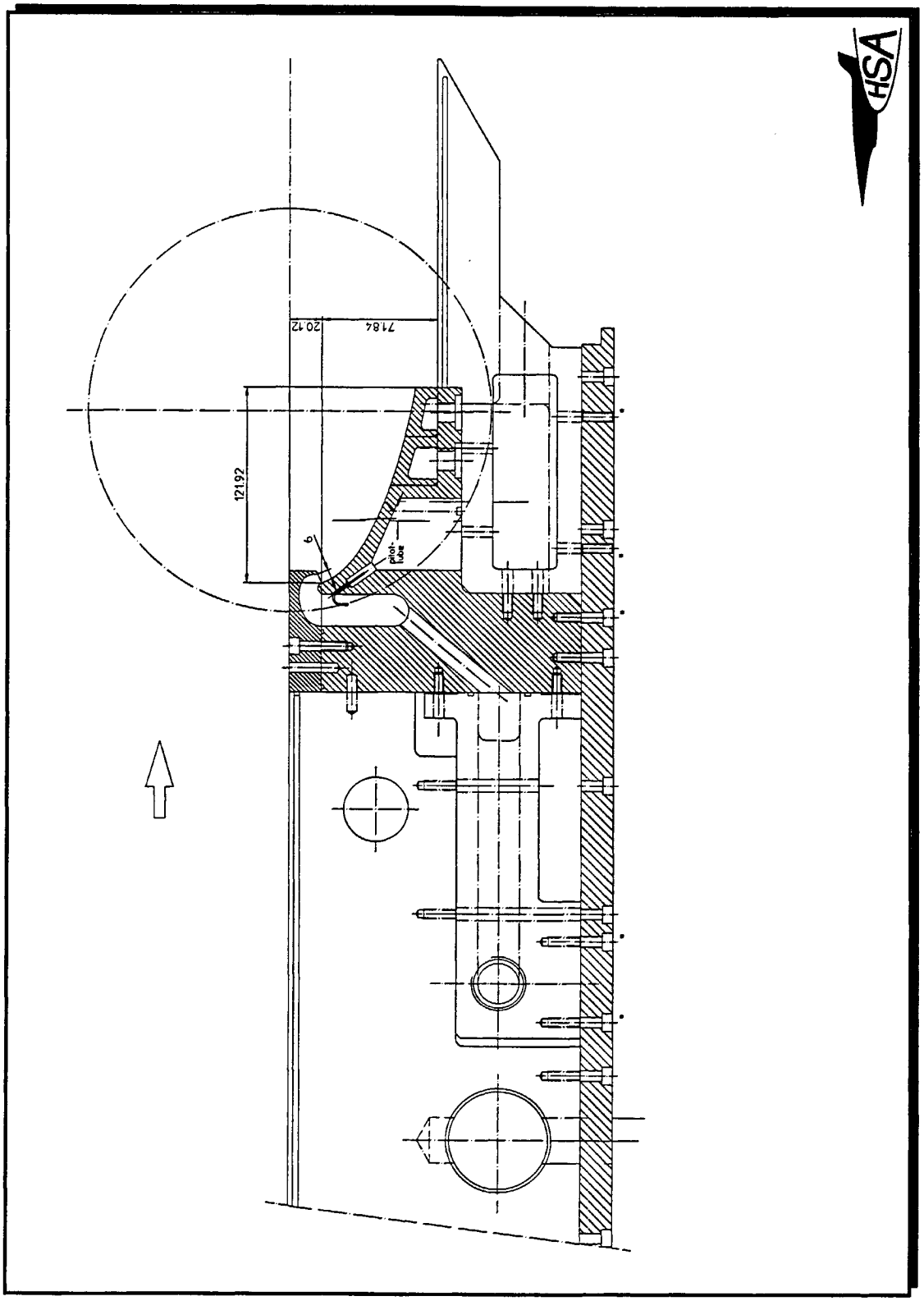

Figure 4: Plug Nozzle Model Showing Exhaust Nozzle and Some Construction Details

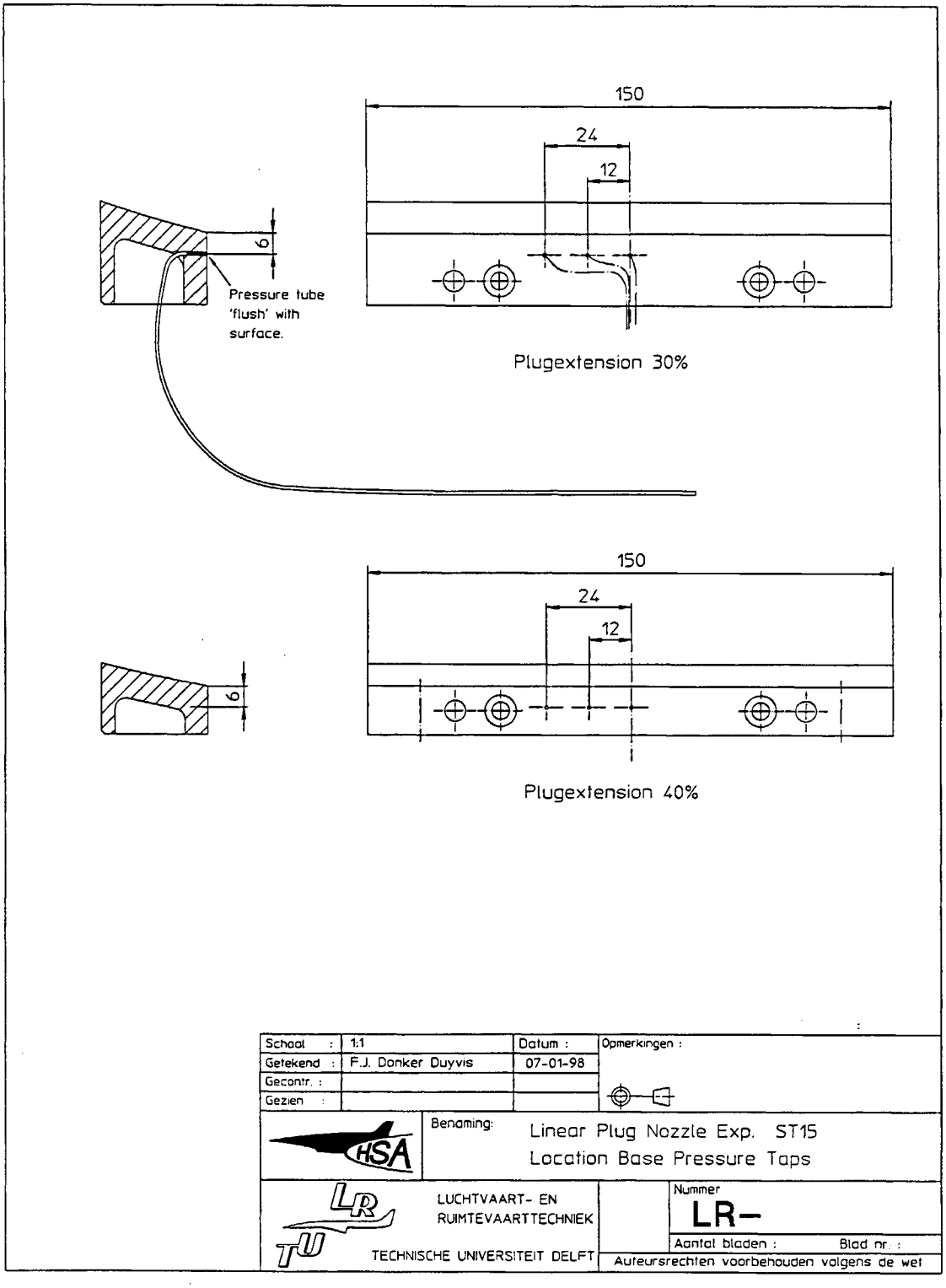

Figure 5: Location of Pressure Taps along Nozzle Base

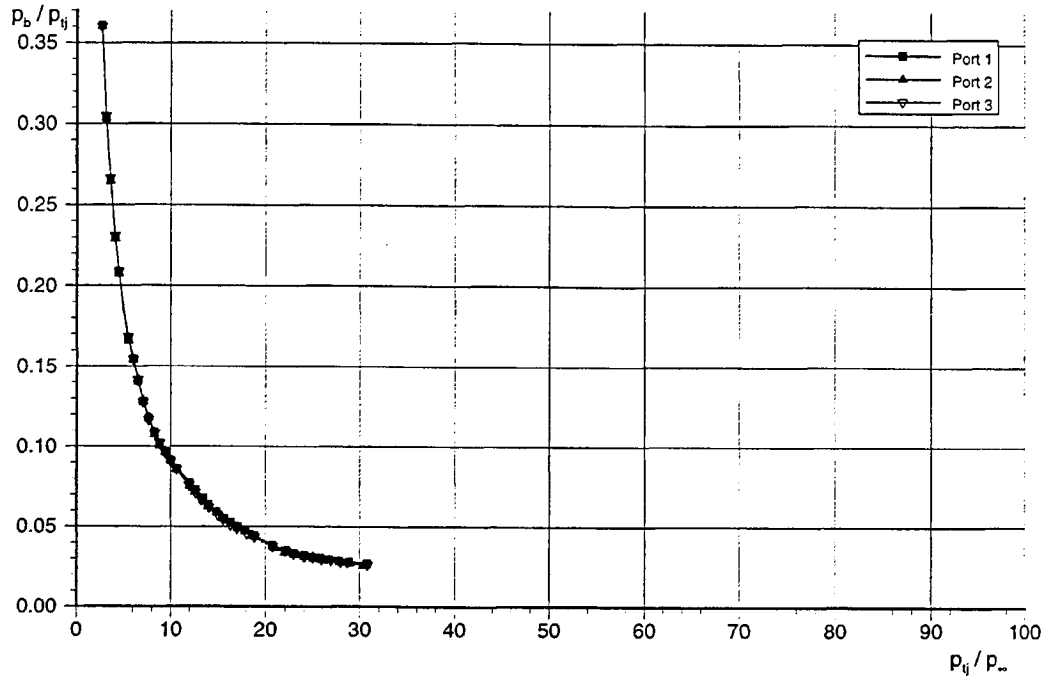

Figure 6: p_b/p_{t_j}-p_{t_j}/p_∞ curve, $M_\infty = 0$, 30% Plug-length

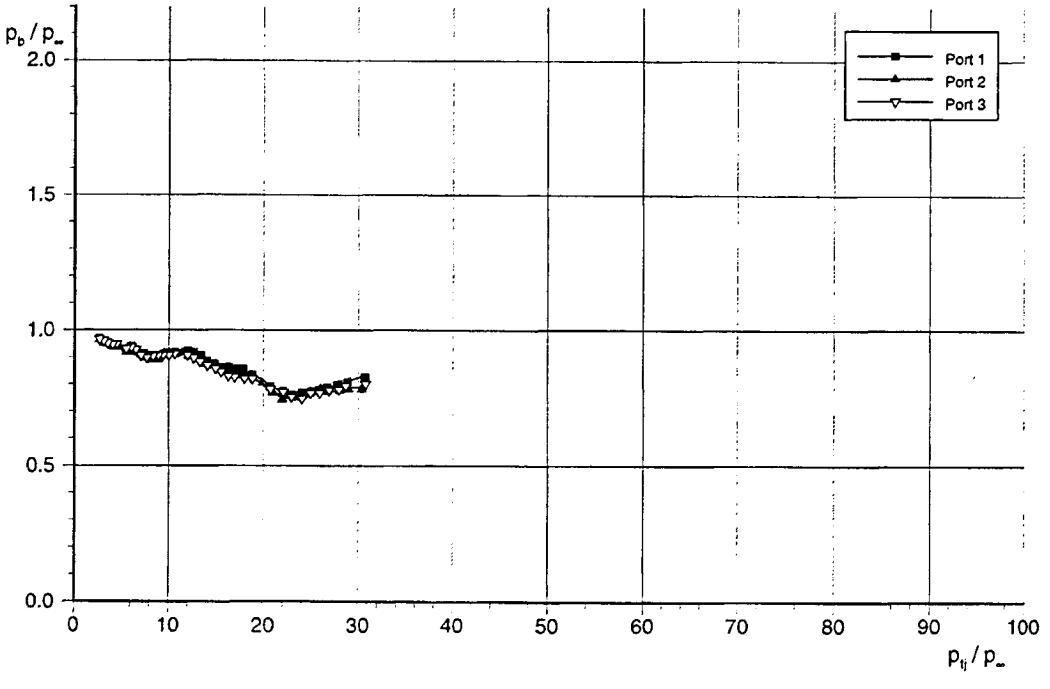

Figure 7: p_b/p_∞-p_{t_j}/p_∞ curve, $M_\infty = 0$, 30% Plug-length

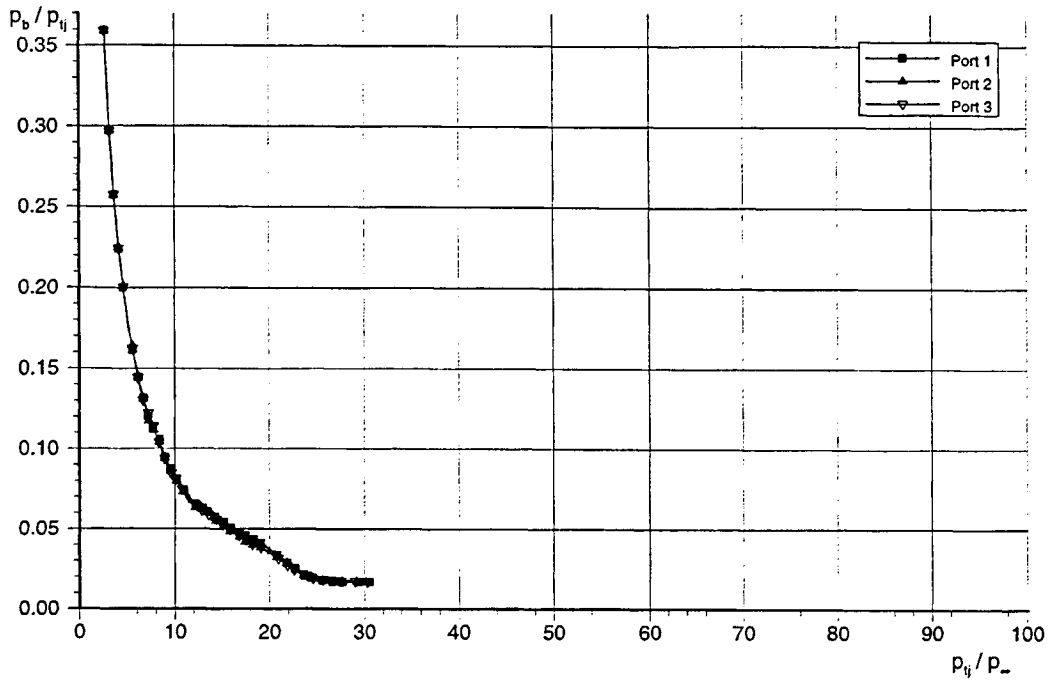

Figure 8: p_b/p_{t_j}-p_{t_j}/p_∞ curve, $M_\infty = 0$, 40% Plug-length

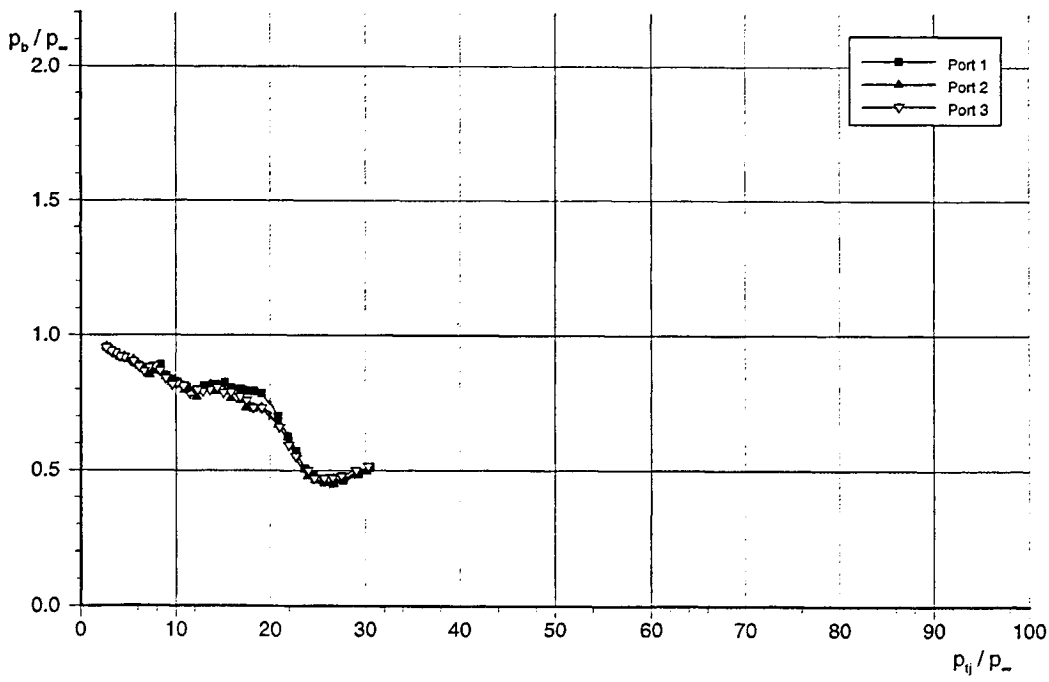

Figure 9: p_b/p_∞-p_{t_j}/p_∞ curve, $M_\infty = 0$, 40% Plug-length

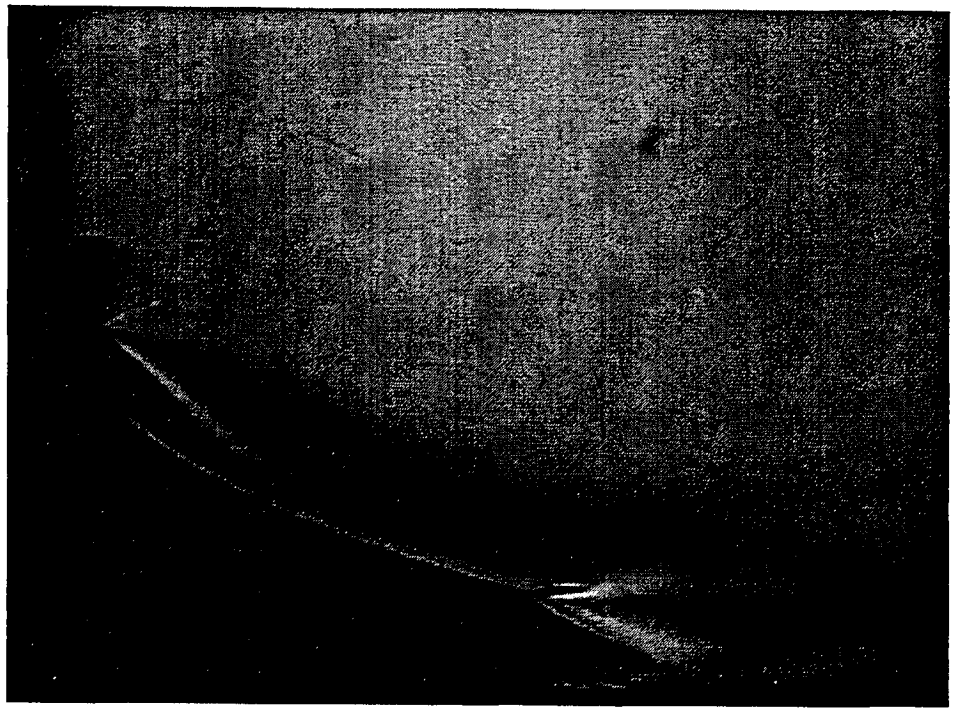

Figure 10: Schlieren-photograph, $M_\infty = 0$, $p_{t_j}/p_\infty = 22.1$, 30% Plug-length

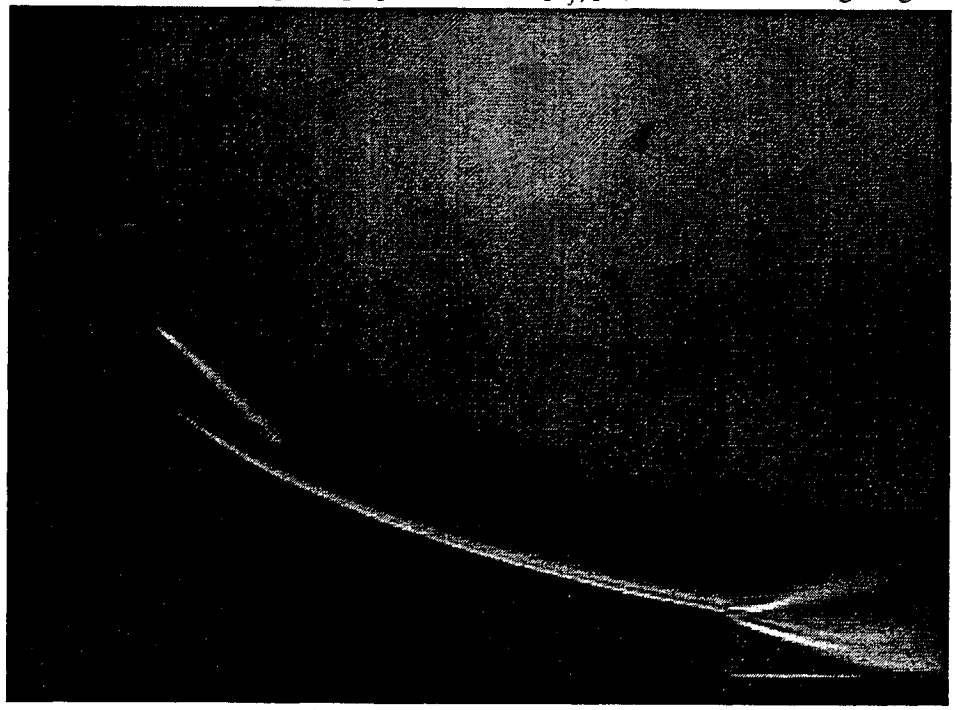

Figure 11: Schlieren-photograph, $M_\infty = 0$, $p_{t_j}/p_\infty = 19.6$, 40% Plug-length

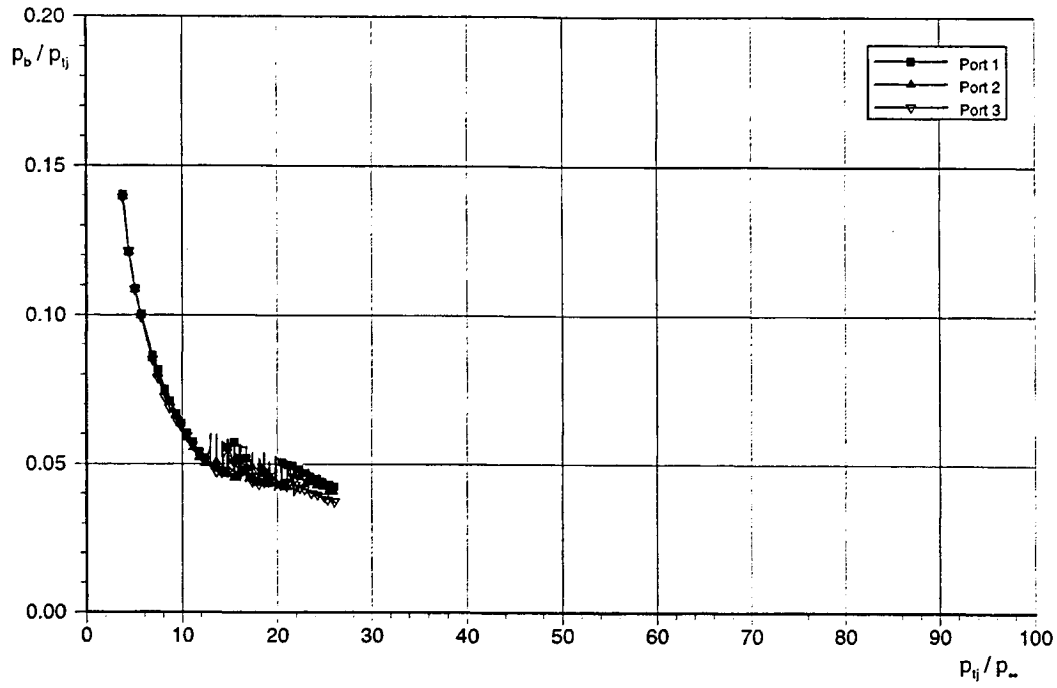

Figure 12: p_b/p_{t_j}-p_{t_j}/p_∞ curve, $M_\infty = 1.5$, 30% Plug-length

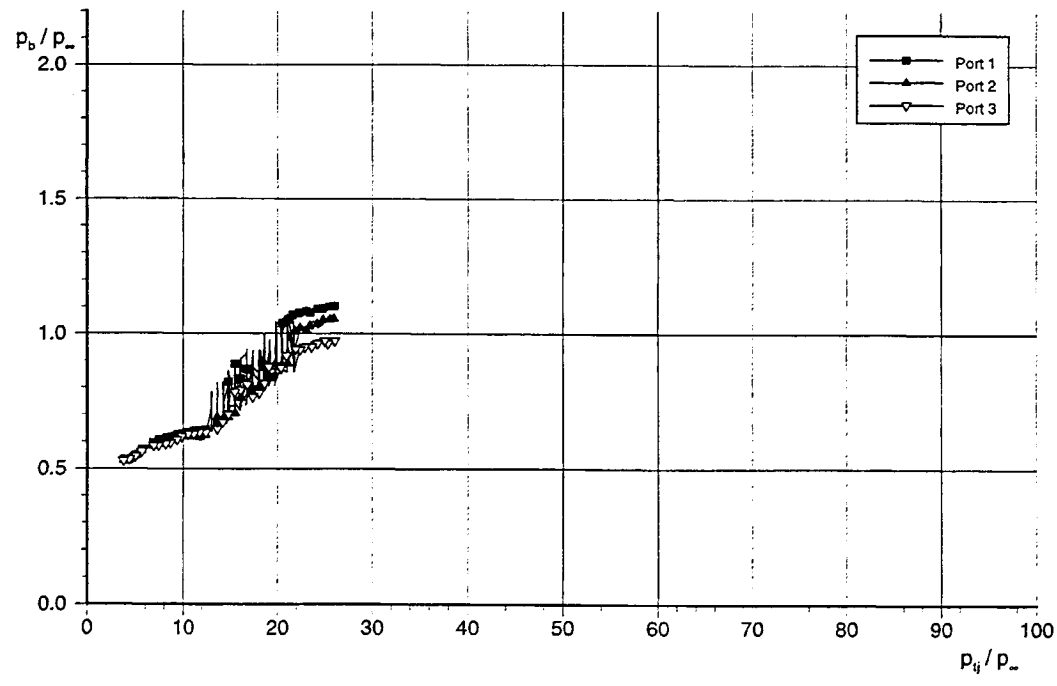

Figure 13: p_b/p_∞-p_{t_j}/p_∞ curve, $M_\infty = 1.5$, 30% Plug-length

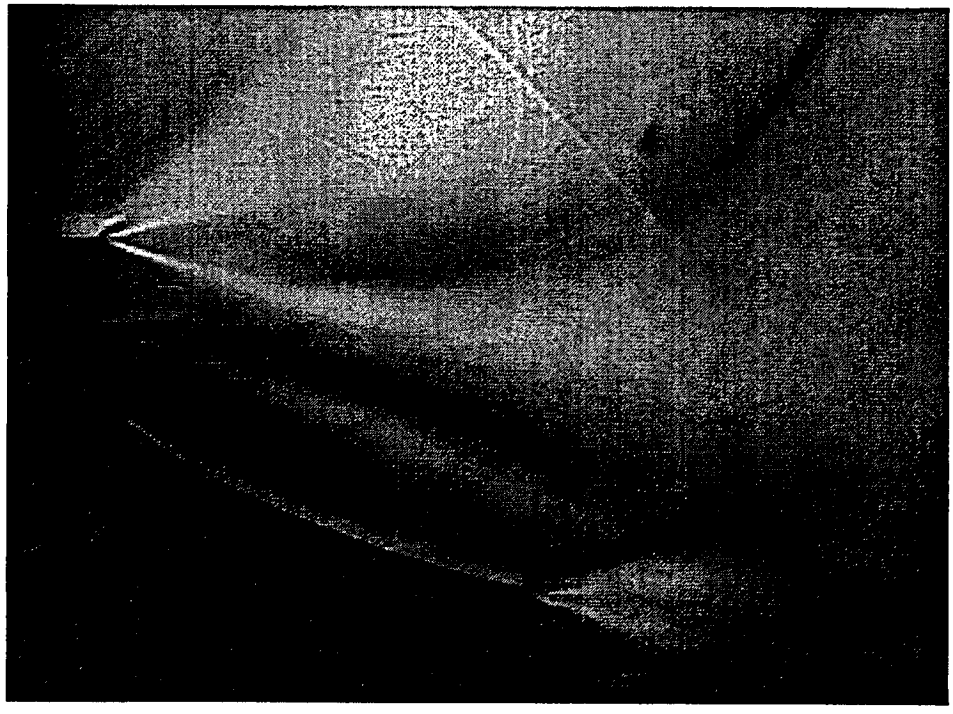

(a) $p_{t_j}/p_\infty = 25.4$

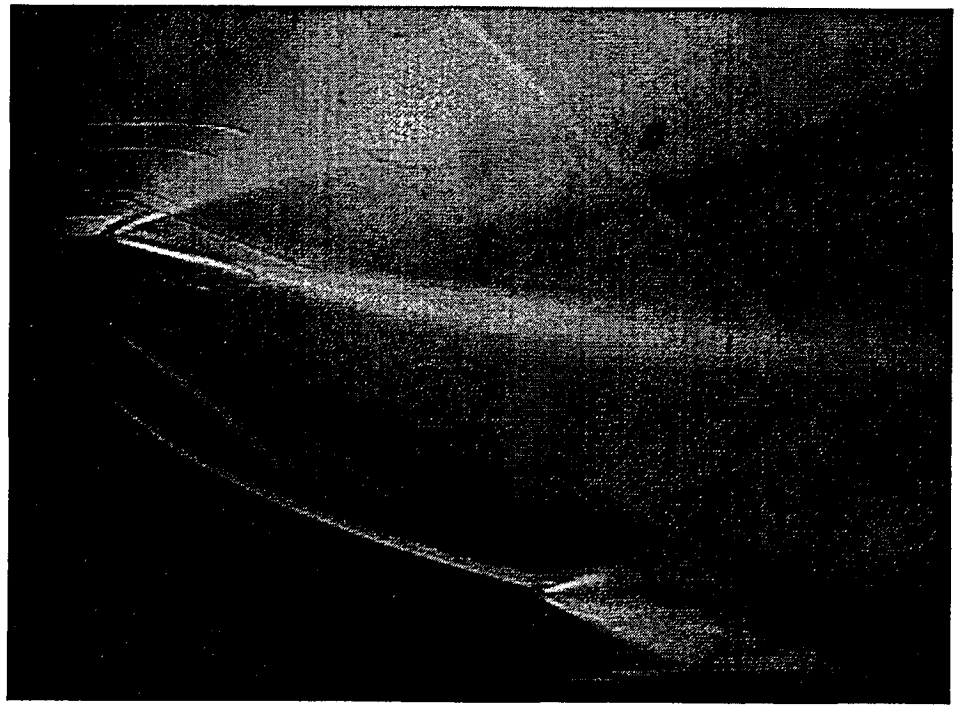

(b) $p_{t_j}/p_\infty = 12.3$

Figure 14: Schlieren-photographs, $M_\infty = 1.5$, 30% Plug-length

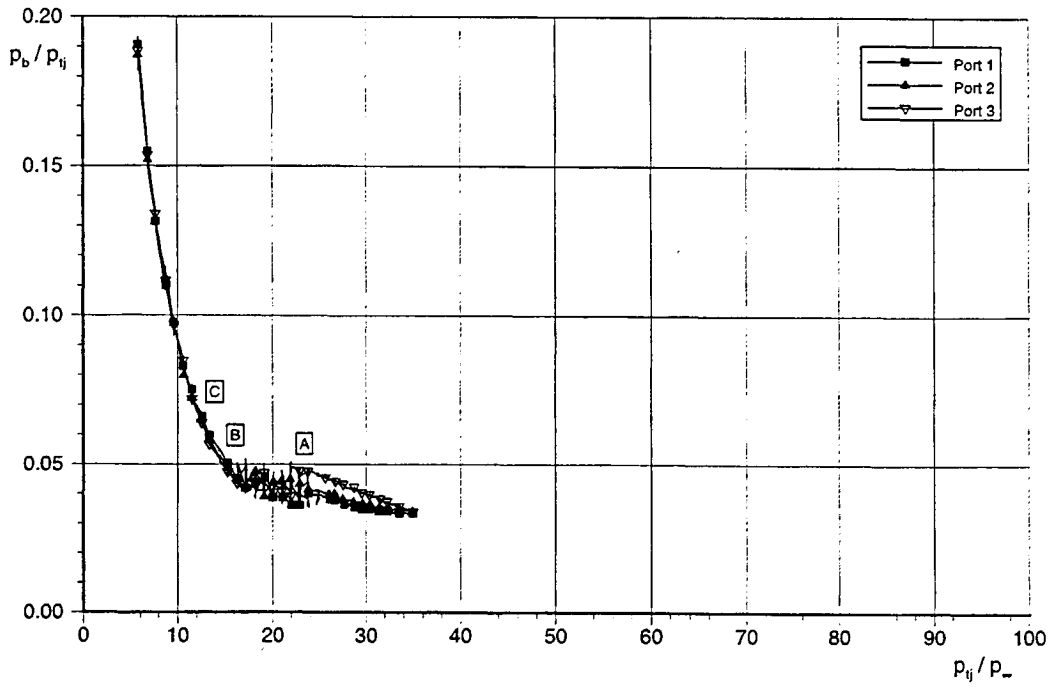

Figure 15: p_b/p_{t_j}-p_{t_j}/p_∞ curve, $M_\infty = 1.5$, 40% Plug-length

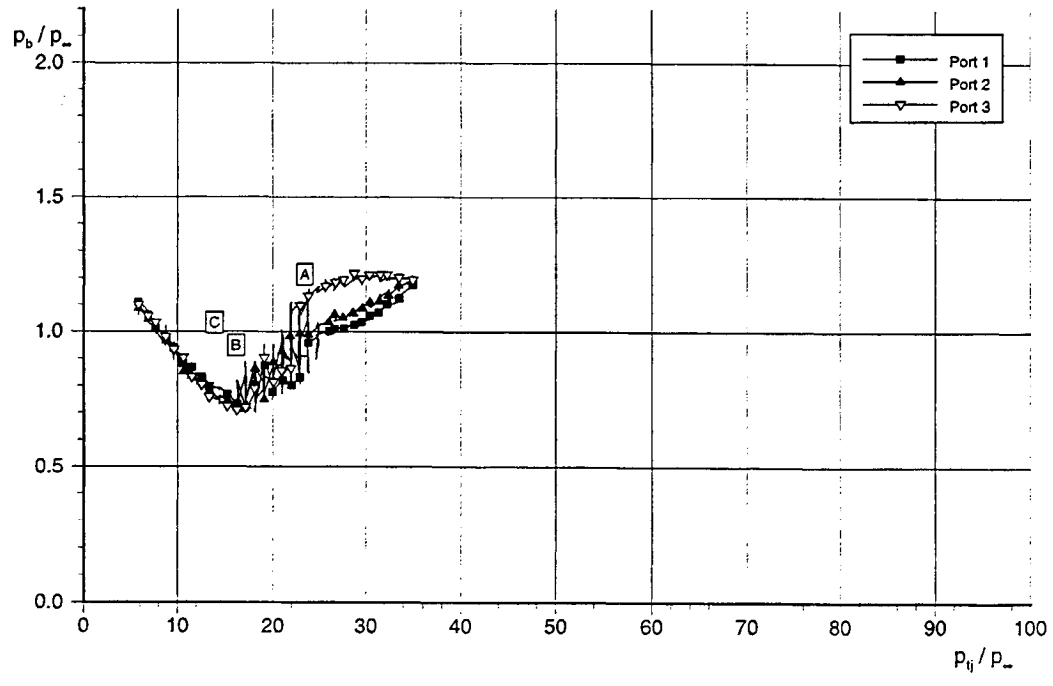

Figure 16: p_b/p_∞-p_{t_j}/p_∞ curve, $M_\infty = 1.5$, 40% Plug-length

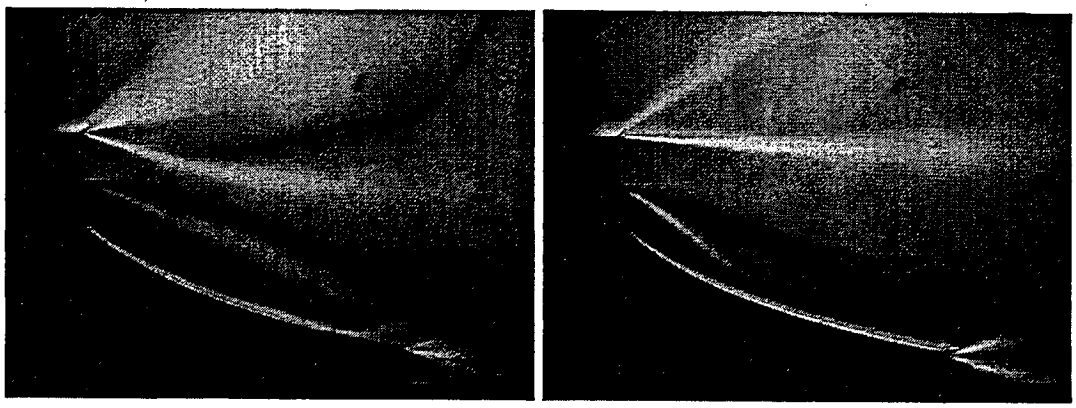

(a) $p_{t_j}/p_\infty = 22.8$, A1

(b) $p_{t_j}/p_\infty = 22.8$, A2

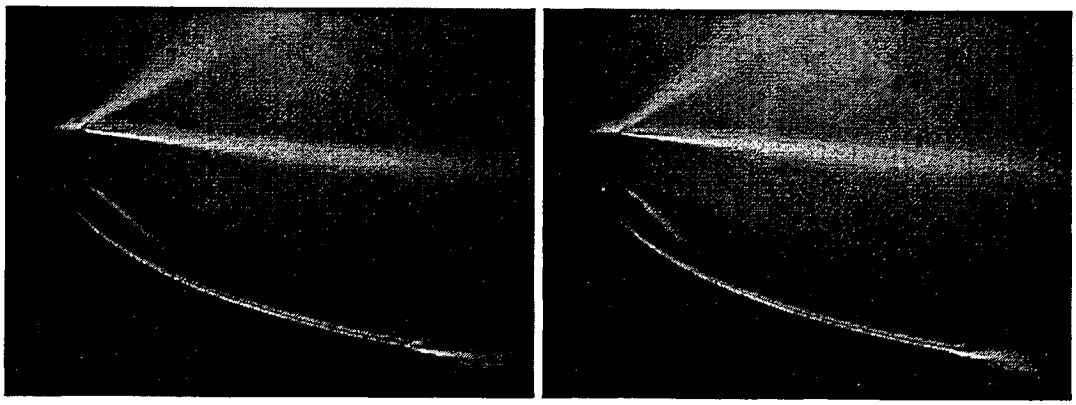

(c) $p_{t_j}/p_\infty = 15.6$, B

(d) $p_{t_j}/p_\infty = 13.3$, C

Figure 17: Schlieren-photographs, $M_\infty = 1.5$, 40% Plug-length

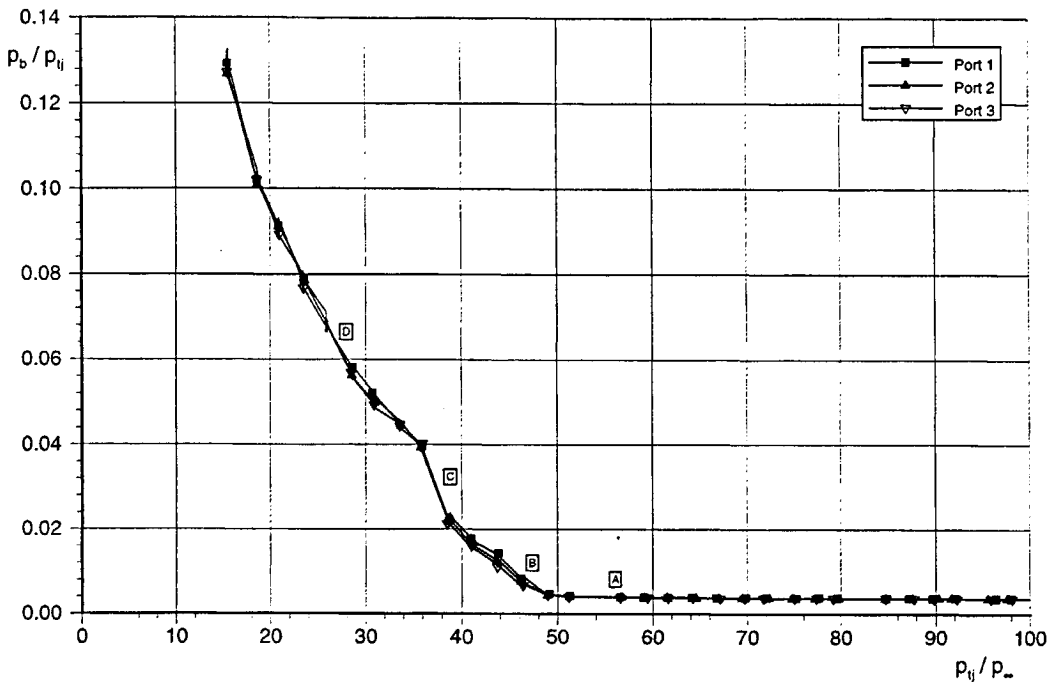

Figure 18: p_b/p_{t_j}-p_{t_j}/p_∞ curve, $M_\infty = 3.0$, 30% Plug-length

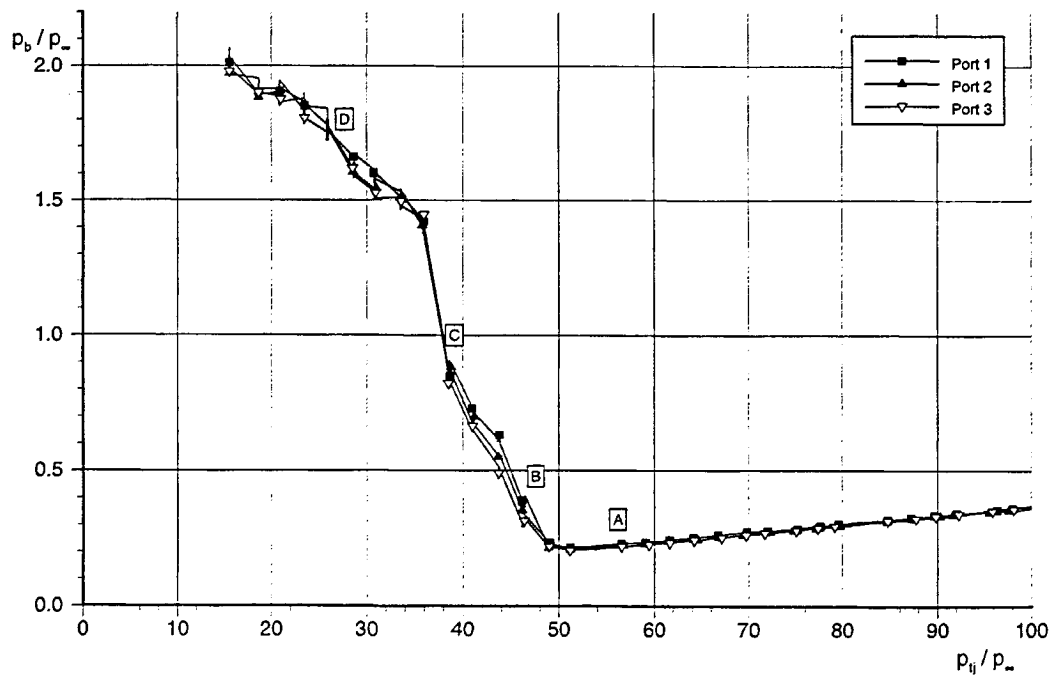

Figure 19: p_b/p_∞-p_{t_j}/p_∞ curve, $M_\infty = 3.0$, 30% Plug-length

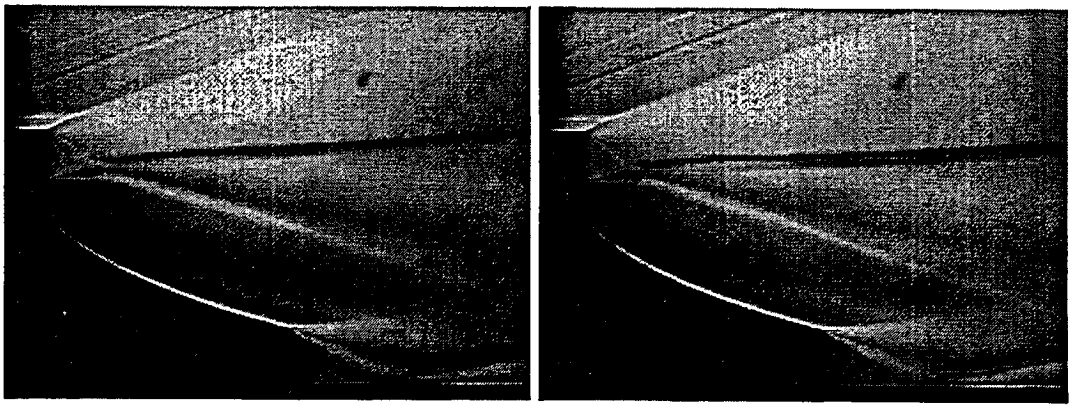

(a) $p_{t_j}/p_\infty = 56.1$, A

(b) $p_{t_j}/p_\infty = 47.3$, B1

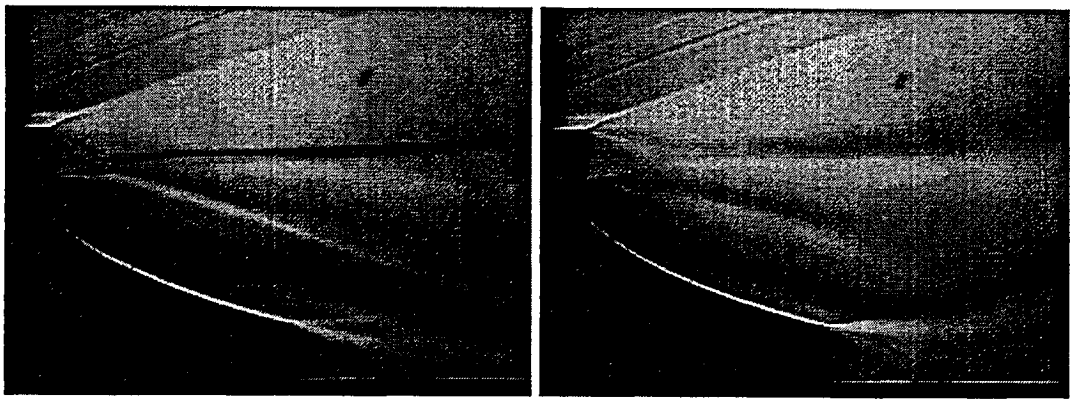

(c) $p_{t_j}/p_\infty = 47.3$, B2

(d) $p_{t_j}/p_\infty = 38.9$, C1

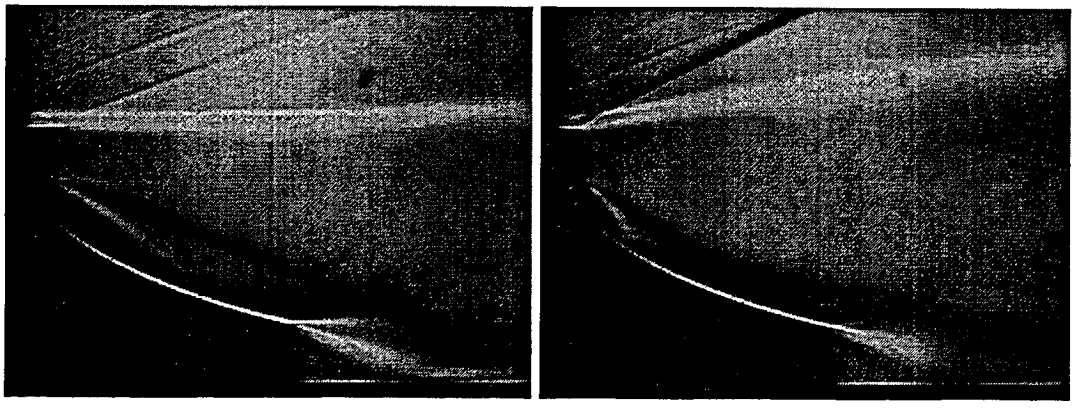

(e) $p_{t_j}/p_\infty = 38.9$, C2

(f) $p_{t_j}/p_\infty = 27.2$, D

Figure 20: Schlieren-photographs, $M_\infty = 3.0$, 30% Plug-length

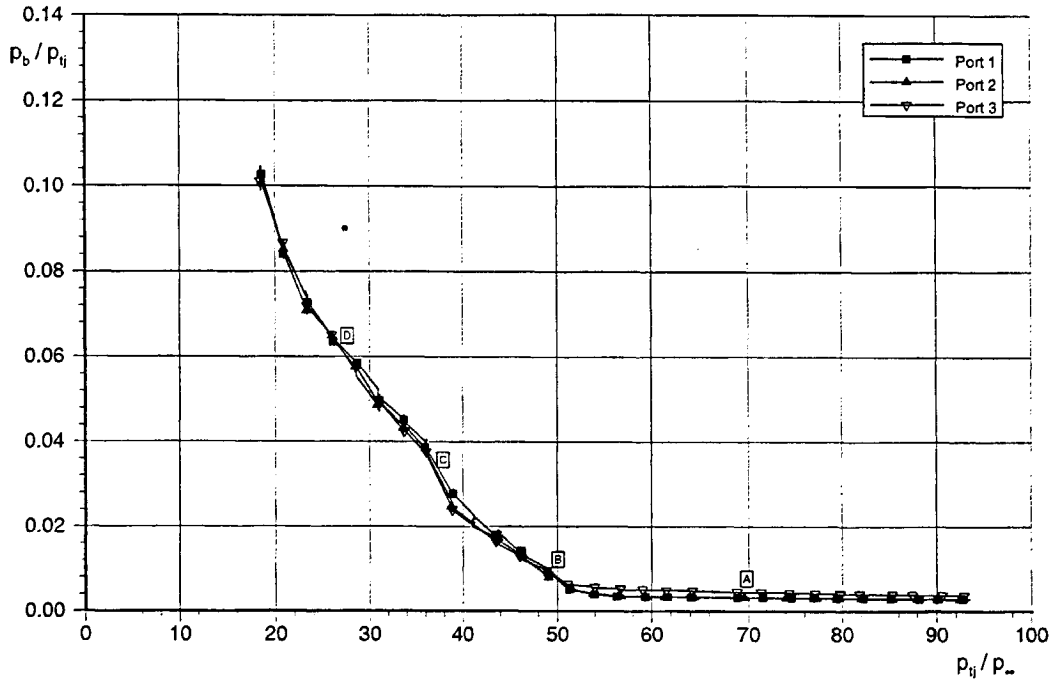

Figure 21: p_b/p_{t_j}-p_{t_j}/p_∞ curve, $M_\infty = 3.0$, 40% Plug-length

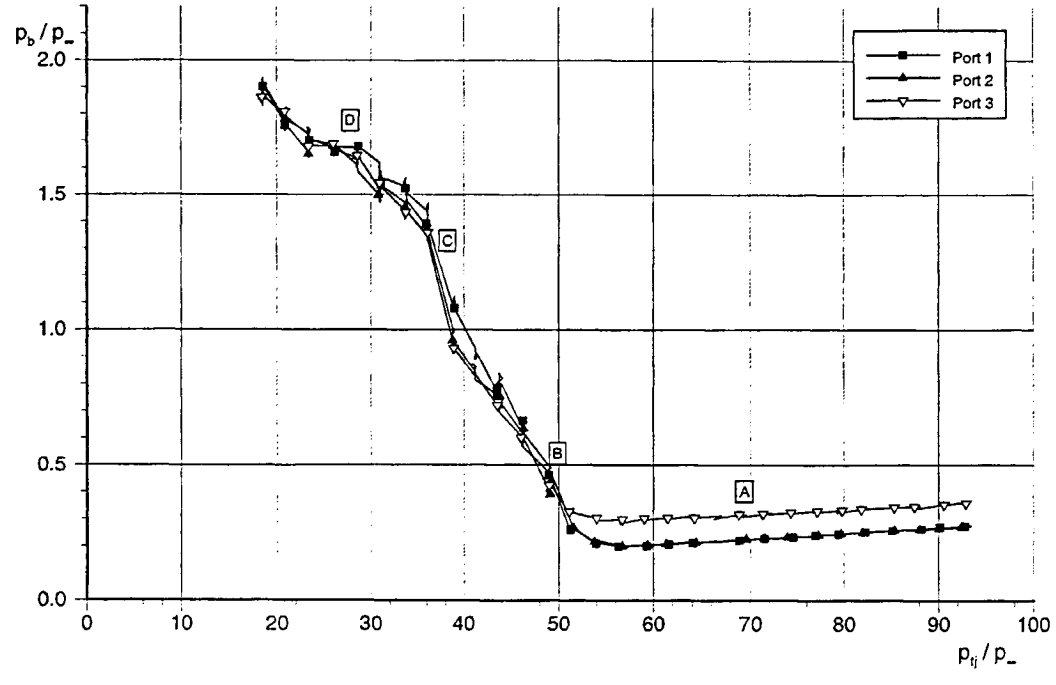

Figure 22: p_b/p_∞-p_{t_j}/p_∞ curve, $M_\infty = 3.0$, 40% Plug-length

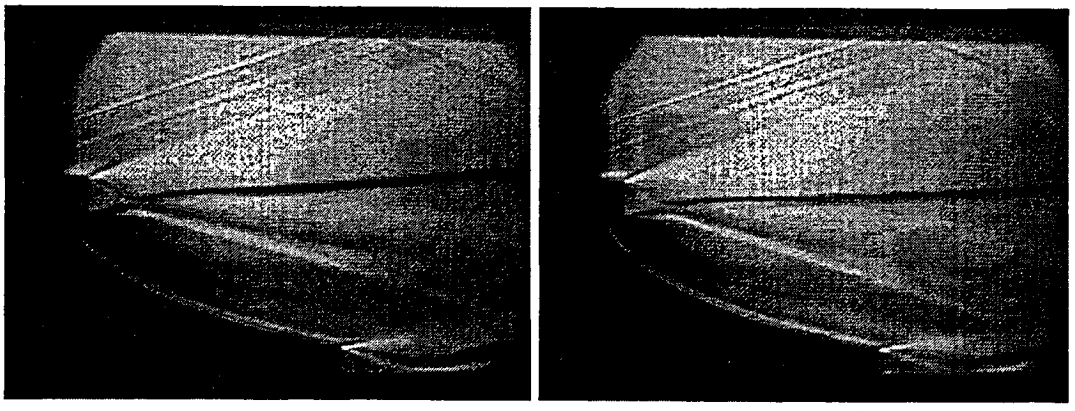

(a) $p_{t_j}/p_\infty = 69.2$, A

(b) $p_{t_j}/p_\infty = 49.6$, B1

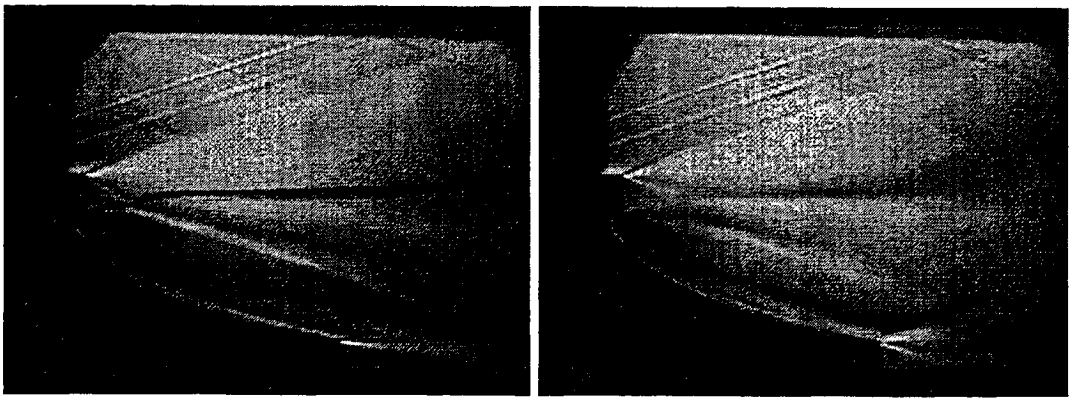

(c) $p_{t_j}/p_\infty = 49.6$, B2

(d) $p_{t_j}/p_\infty = 37.5$, C1

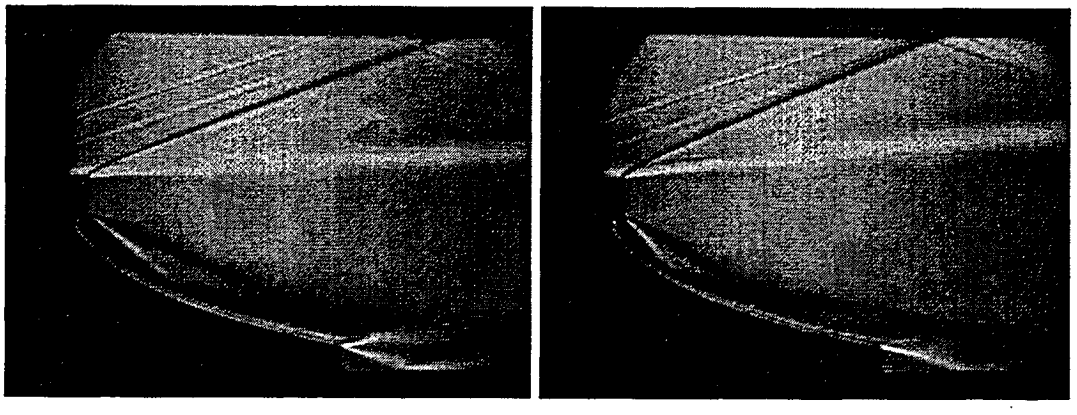

(e) $p_{t_j}/p_\infty = 37.5$, C2

(f) $p_{t_j}/p_\infty = 27.3$, D

Figure 23: Schlieren-photographs, $M_\infty = 3.0$, 40% Plug-length

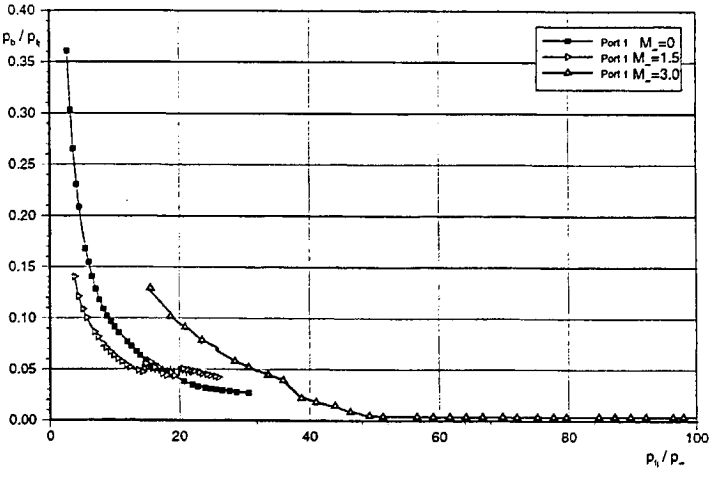

(a) 30% Plug-length

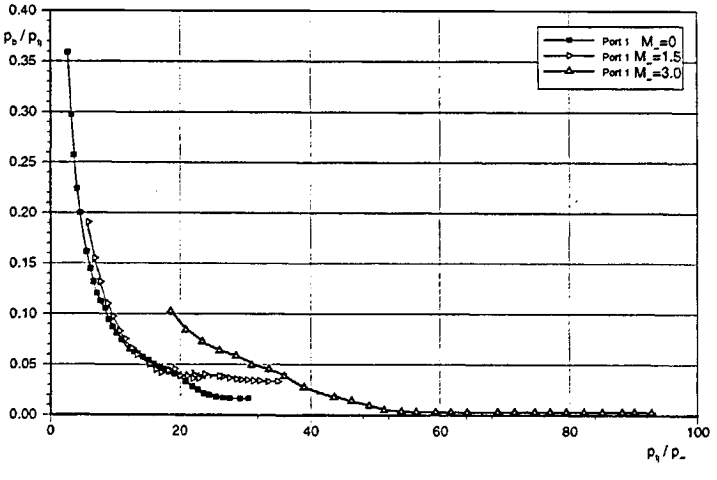

(b) 40% Plug-length

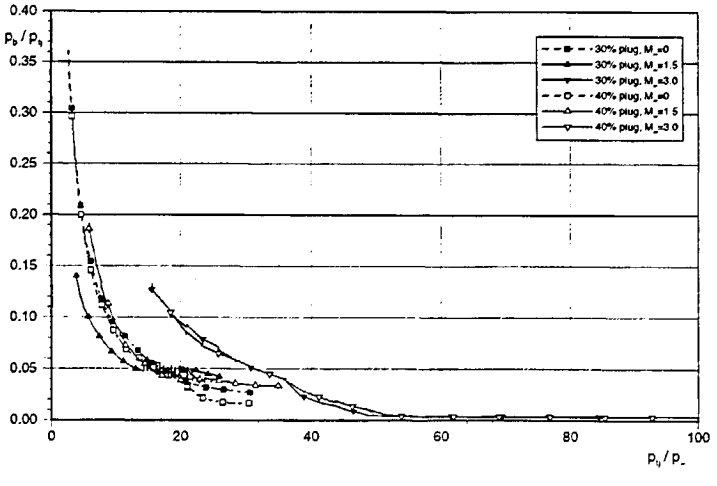

(c) 30% & 40% Plug-length

Figure 24: p_b/p_∞-p_{t_j}/p_∞-curves, Compilation